ORIGINAL ARTICLE

OPEN ACCESS

Non-Newtonian Fluid Flow with Bioconvection: The Role of Rayleigh Number and Buoyancy Over a Sheet.

Jawad Ahmad Jugnoo [1], Amad ur Rehman [2], Talal Taha [3]

Authors' Affiliation:

[1]Department of Civil Engineering, National University of Science & Technology (NUST), Islamabad, Pakistan
Email: jawadjugnoo55@gmail.com

[2]Department of Mathematics and Statistics, International Islamic University (IIU), Islamabad, Pakistan
Email: amad.phdma131@iiu.edu.pk

[3]Department of Mathematics and Statistics, International Islamic University (IIU), Islamabad, Pakistan
Email: talaltaha1998@gmail.com

Article History:

Submitted: February 22, 2024
Revised: May 27, 2024
Accepted: June 16, 2024
Published online: June 30, 2024

Corresponding author(s):

Amad ur Rehman
amad.phdma131@gmail.com

A B S T R A C T

This study investigates the effects of magnetohydrodynamics (MHD) and bioconvection on Casson-Williamson nanofluid flow along a stretched sheet. Such an analysis of fluid dynamics takes into account the impact of MHD, chemical reactions, and gyrotactic microorganisms. For velocity and magnetic field behavior exploration, the concept of buoyancy ratio has also been proposed in the study. The Casson and Williamson rheological models characterize the fluid properties to understand the effects of these parameters by the motion of motile gyrotactic microorganisms. Similarity variable is used to reduce nonlinear partial differential equations including boundary conditions to strong coupled ordinary differential equations, which are easier to analyze. The solutions can be obtained by the use of `bvp4c', a popular numerical method for nonlinear boundary value problems, which enables sensitivity about fluid dynamics of different physical parameters on profiles of $f'(\eta), \theta(\eta), \varphi(\eta), \varepsilon(\eta), f''(\eta)$ *and* $\theta'(\eta)$.

Numerous physical characteristics, such as the buoyancy ratio, thermophoresis variable, Brownian motion variable, bioconvection number, Eckert number, and thermal radiation, determine the behavior of non-Newtonian fluids. The result shows that the skin friction decreases by increasing the value of the magnetic field the Nusselt number decreases by raising the value of heat generation parameters and the Sherwood number increases by increasing the value of Lewis number. The goal of the study is to notice the impact of buoyancy ratio and Rayleigh number on fluid behavior. The velocity profile declines by increasing the value of N_r and R_b and the temperature profile increases for thermophoresis and Brownian motion parameter value rise.

Keywords: Non-Newtonian Fluid, Bioconvection, Rayleigh Number, MHD, motile gyrotactic, and Casson-Williams nanofluid.

(MSC2020) Codes: 76A05, 76D27, 76R50, 76Z05, 76D08, 76D99

1 | INTRODUCTION

To analyze the impact of heat and mass transfer over a stretching sheet. The combination of two non-Newtonian fluids makes the problem complex. The use of non-Newtonian fluid along sheet is listed real engineering model. To comprehend the aerodynamic behavior of greater surfaces, such as turbine shafts and Aeroplan wings, sheets that resemble thin flat plates are examined. This aids in creating surfaces that maximize lift and reduce drag. In wind tunnels, thin sheets are utilized to simulate particular flow paths and investigate various flows related to materials, a significant topic in the fields of aviation and automotive technology. The thin layer of viscous fluid flows in a way that prevents turbulence known as laminar sheet flow. The principles guiding the movement of fluid in thin films are essential to determining these properties studied in [1]. They discovered that for any value of the variables, the decreased Sherwood number is a rising function, and the decreased Nusselt number is a declining function examined in [2]. Explored the impact of N_t and N_b rise, the decreased Shx, and growth for unchanged Pr, Le, and Bi whereas the decreased Nusselt number drops in [3]. They examined the HAM was used to analyze the analytical solution. The results indicated that the solution relies on the following numbers Pr, Le, N_b, and N_t in [4]. It assessed those greater values of γ and Pr cause a thermal layer to increase, instead higher numbers of Ec and N_t cause the thermal thickness to decrease investigated in [5].

2 | LITERATURE REVIEW

Magnetohydrodynamics is the science that deals with the study of the dynamics of electrically conducting fluids under the influence of magnetic fields. This affects flow behavior and heat transfer. Bioconvection is the self-organized motion of microorganisms in a fluid and produces patterns and nutrient transport because of their motility. Casson-Williamson fluid, sometimes known as a non-Newtonian fluid with yield stress and shear-thinning properties, combines properties from Casson fluid and Williamson fluid. They investigated the analytical solutions for the simulated problem by using HAM. The pair stress factor grows substantially with the rising microstructural slip component in the first two scenarios where n=0 and n=0.5. On the other hand, a decreasing influence on pair stress is shown in the third scenario n=1 in [6]. They explored the heat boundary layer levels grow with greater magneto coefficients but momentum across the x and y directions declines studied in [7]. Using a shooting technique based on RK, computational solutions are produced for the developing concern. The impact of buoyancy force present in non-Newtonian fluid is analyzed in [8]. It is observed that as radiation obstacles increase, the flow and temperature curves increase. It determined the dual solution and studied that by raising the chemical reactions variable, the mass flow at the wall increases. As λ and N are larger, the velocity curve improves in the top section approach in [9]. Evaluated these urging engineers and scientists to employ alternative methods when buoyancy-driven fluids are produced by significant temperature variations, as opposed to the Bossiness approximation's limited range of accuracy [10]. Focused the most potent Shooting process used to compute the changed system numerically. The fluid's thermal measure increases as the buoyancy factor rises [11]. The ambient temperature should be determined using the BEM and integrated into CFD simulations. With an emphasis on modeling and controlling the buoyancy impact on airflow velocity, the investigation examined current achievements in the field of buoyancy effect studies in metropolitan ventilation [12]. It explored the nonlinear convection factor rises, the flow speed climbs close to the surface, and falls farther from it [13]. This kind of flow is helpful for numerous manufacturing processes, including nuclear energy, photovoltaic arrays, combustion engine living things, the polymeric sector, and the chilling process of technology.

The study of non-Newtonian fluids is becoming rapidly important in the food industry, pharmaceuticals, and materials manufacturing, where the complexity of flow behavior can make all the difference between the successful accomplishment of mixing, pumping, and heat transfer processes. Bioconvection, through the movement of microorganisms, is also one of the key contributors to the transport of nutrients within aquatic ecosystems and engineered systems such as bioreactors. The results of the present study are crucially presented as how interaction can significantly impact both thermal management and fluid transport due to changes in non-Newtonian fluid behavior and bioconvection. The influence of varying viscosity results in a dip in the speed trajectory, but the recorded influence of the Casson fluid on the flow rate shows an increase in fluid velocity. The greater production of heat and thermal conductivity coefficients caused an improvement in heat distributions investigated in [14]. Examined a greater velocity profile produced by greater values of Gr and Gm. Speed fluid is seen to decline or slow down as Pr and Sc levels rise. The velocity curve exhibits a declining tendency as the Casson flow coefficient rises. The fluid temperature increases when radiation characteristics are present [15]. They noticed the declining behavior of gyrotactic microorganisms by using LMS. Furthermore, the outcomes indicate that thermal curves increase with increasing radiation coefficients examined in [16]. It investigated the velocity decreases as the permeability variable, the magneto, or the fluids variable increases. When the Pr rises, the heat flux and related layer depth fall in [17]. Thermal transfer and fluid movement enhance with a rise in the Casson variable. The Da and β variables all cause the Nusselt value to behave in a rising manner discovered in [18]. Both observed that when heat radiation rises, velocity rises, and thermal falls. The relative impact of conductive heat transmission on thermal energy transport is shown by the radiation coefficient. Concentration tends to fall as the chemical reaction factor increases [19]. It demonstrates that the velocity curves are improved by the Ha variables. Furthermore, the thermal value falls with increasing Ha numbers conversely, decreasing numbers have the opposite impact in [20]. The studied Nusselt number shows an inverse trend from the skin friction value which increases as the magnetic field's variable, the permeability variable grows discussed in [21]. The primary goal to determine its behavior is influenced by variations in the Rayleigh and Hartmann values in various topologies. When the heat factor increases, the Nusselt value exhibits a rising behavior analyzed in [22]. Noticed the velocity distribution of Williamson increased with variations in the dimensional length variable over a sheet in [23]. Shows that when the total fraction of the nanotubes in a truncated cone increase, the depth layer of heat reduces [24]. Determined that computationally thermal transmission properties are examined with various physical variables across a cylinder in [25]. They explored by an increasing Hartmann amount, it has been seen that thermal transmission and total entropy exhibit falling behavior in [26]. The execution of a variational repetition approach is the foundation of the computational methods studied in [27]. It is observed that when the thermal source variables are exponential a heat curve rises. Suggested that when the magnetic values are raised, there is a decline in velocity and a heat rise. The thermal curves get flatter as the Radiation factor above a plate is observed in [28]. Analyzed there is an obvious rise in the buoyancy relation to fluid flow and skin friction value for the curved factor decreases. The radiation factor increases the rate of heat transmission studied in [29]. Investigated whether there is resistance in the fluid movement with a longer pause when there are larger Williamson fluid parameters involved. Consequently, near the bottom edge of the channel, the flow dispersion decreases examined in [30]. It was discovered at small magnetic factor levels, the Weissenberg value has favorable sensitivity; at moderate to high magneto-factor levels, it exhibits adverse sensitivity [31]. Explored numerous amounts for key factors that have been shown in statistical bar charts for the investigation of the Skin friction factor, Nusselt, and Sherwood factor in [32].

The author has studied the flow dynamics of Casson-Williamson nanofluids under the influence of non-Newtonian fluids, combined effects of MHD and bioconvection, etc. Much work in literature is yet to be explored on the mutual interaction of their parameters, effects of chemical reactions, and gyrotactic microorganisms. A more significant part of critical parameters, such as the impact of the buoyancy ratio and the effects of the Rayleigh number on the velocity and thermal profiles, are yet to be studied in this regard. In this paper, we intend to fill these gaps by analyzing the interaction of these variables in Casson-Williamson nanofluid flow along a stretched sheet, providing valuable insights toward practicing applications in various fields of engineering.

2.1 | Problem Statement

The incompressible steady flow mixed with bioconvection and chemical reaction with Casson - Williamson fluid over a slippery sheet has been considered for analysis. While the induced magnetic field disregards the unified magnetic field anticipated along the vertical axis, it is expected that the magnetic Reynold value is exceedingly small. The process of flow along the mathematical model and cartesian position are shown in Figure 1. The Casson-Williamson model may be used to describe these fluids consequently.

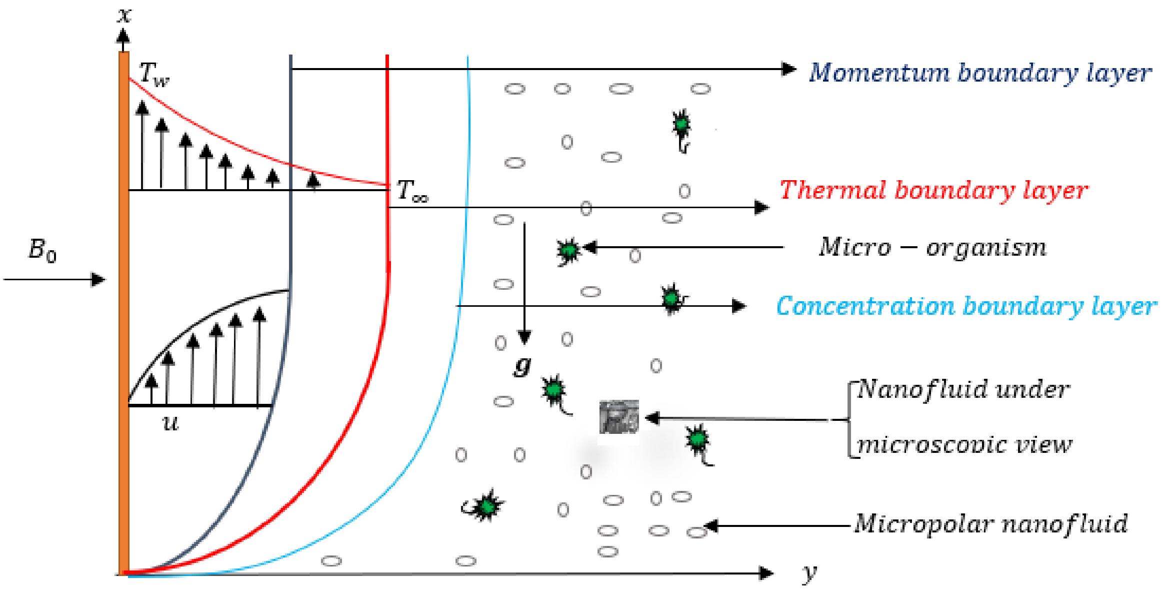

Figure 1. Flow Problem

$$\tau_{ij} = \left(1+\frac{1}{\beta}\right)\frac{\partial u}{\partial y} + \frac{\Gamma}{\sqrt{2}}\left(\frac{\partial u}{\partial y}\right)^2 \tag{1}$$

Where β and Γ is a Casson or Williamson parameters. The governing equation is considered from [33], [34].

$$\frac{\partial u^*}{\partial x} + \frac{\partial v^*}{\partial y} = 0, \tag{2}$$

$$u^*\frac{\partial u^*}{\partial x} + v^*\frac{\partial u^*}{\partial y} = \vartheta\left(1+\frac{1}{\beta}\right)\frac{\partial^2 u^*}{\partial y^2} + \sqrt{2}\vartheta\Gamma\frac{\partial u^*}{\partial y}\frac{\partial^2 u^*}{\partial y^2} - \frac{\sigma B^2 u^*}{\rho} - \frac{\vartheta}{k}u^* + \frac{1}{\rho_f}\left[(1-C_f)\rho_f\beta g(T^* - T_\infty) - g(\rho_p - \rho_f)(C^* - C_f) - \gamma^* g(n^* - n_\infty)(\rho_m - \rho_f)\right], \tag{3}$$

$$u^*\frac{\partial T^*}{\partial x} + v^*\frac{\partial T^*}{\partial y} = \frac{k}{\rho c_p}\left(1+\frac{16\sigma^* T_\infty^3}{3kk^*}\right)\frac{\partial^2 T^*}{\partial y^2} + \tau\left[D_B\frac{\partial C^*}{\partial y}\frac{\partial T^*}{\partial y} + \frac{D_T}{T_\infty}\left(\frac{\partial T^*}{\partial y}\right)^2\right] + \frac{\mu}{\rho C_p}\left[\left(1+\frac{1}{\beta}\right)\left(\frac{\partial u^*}{\partial y}\right)^2 + \frac{\Gamma}{\sqrt{2}}\left(\frac{\partial u^*}{\partial y}\right)^3\right] + \frac{Q_o}{\rho c_p}(T^* - T_\infty), \tag{4}$$

$$u^*\frac{\partial C^*}{\partial x} + v^*\frac{\partial C^*}{\partial y} = D_m\frac{\partial^2 C^*}{\partial y^2} + \frac{D_T}{T_\infty}\frac{\partial^2 T^*}{\partial y^2} - K_r(C^* - C_\infty), \tag{5}$$

$$u^*\frac{\partial n^*}{\partial x} + v^*\frac{\partial n^*}{\partial y} + bW_c\frac{\partial}{\partial y}\left(\frac{n^*}{\Delta C}\frac{\partial C^*}{\partial y}\right) = D_m\frac{\partial^2 n^*}{\partial y^2}. \tag{6}$$

The T is the nanofluid temperature, C is the nanofluid concentration, *and* u and v are the nanofluid velocity components. The thermal conductivity k and ρ density is supposed to be constant.

The boundary condition for the above problem is taken [33], [34].

$$u^* = ax + \lambda_1 \left[\left(1 + \frac{1}{\beta}\right) \frac{\partial u^*}{\partial y} + \frac{\Gamma}{\sqrt{2}} \left(\frac{\partial u^*}{\partial y}\right)^2 \right], v^* = 0, T^* = T_w, C^* = C_w, n^* = n_w \ \ at\ y = 0, \tag{7}$$

$$u^* \to 0,\ T^* \to T_\infty,\ C^* \to C_\infty,\ n^* \to n_\infty \ \ at\ y \to \infty .$$

Where β is the Casson parameter, g is the gravitational acceleration parameter, σ^* is the Stefan-Boltzmann constant, D_B is the Brownian diffusion coefficient, D_T is the thermophoretic diffusion coefficient, k^* is the absorption coefficient, K_r is the chemical conversion rate, Q_o is the heat absorption coefficient, C_∞ is concentration parameter. , σ is the nanofluid electrical conductivity, ϑ is kinematic viscosity, ρ_f, ρ_p, ρ_m is nanofluid density, B is a magnetic field, λ_1 ia slip velocity factor, D_m id Diffusion coefficient of motile density, b is chemotaxis constant, W_c is the swimming speed of a cell, C_w, T_w, n_w are a surface concentration of nanoparticles, surface temperature, and surface concentration of microorganisms. The C_∞, T_∞ and n∞ is the ambient concentration of nanoparticles, ambient temperature, and ambient concentration of microorganisms, and g is the gravitational constant. To convert PDEs into ODEs by using this similarity variable and new boundary conditions corresponding to these ODEs. The similarity transformation is chosen from [33-34]

$$\eta = \sqrt{\frac{a}{\vartheta}}y,\ \ u^* = axf'(\eta),\ \ v^* = -\sqrt{a\vartheta}\mathrm{f}(\eta),\ \ \theta(\eta) = \frac{T^*-T_\infty}{T_w-T_\infty}\ ,\varphi(\eta) = \frac{C^*-C_\infty}{C_w-C_\infty}\ ,\ \varepsilon(\eta) = \frac{n^*-n_\infty}{n_w-n_\infty}. \tag{8}$$

Applying this similarity variable of equation (8) to reduce the equation (3)-(7)

$$\left(1 + \frac{1}{\beta}\right) f''' + W_e f'' f''' - f'^2 - k_p f' - Mf' + \lambda(\theta - N_r\ \varphi - R_b \varepsilon) = 0, \tag{9}$$

$$\frac{1}{P_r}(1 + R)\theta'' + N_b \theta' \varphi' + N_t \theta'^2 + E_c \left[\left(1 + \frac{1}{\beta}\right) f''^2 + \frac{W_e}{2} f'''^3\right] + Q\theta + f\theta' = 0, \tag{10}$$

$$\varphi'' + \frac{N_t}{N_b}\theta'' - GS_c\varphi + S_c f \varphi' = 0, \tag{11}$$

$$\varepsilon'' - L_b(f'\varepsilon - f\varepsilon' + Bf') - P_e(\varphi''(\varepsilon + \Omega) + \varepsilon'\varphi') = 0, \tag{12}$$

The corresponding boundary condition of ODEs

$$f'^{(\eta)} = 1 + \lambda_1 \left[\left(1 + \frac{1}{\beta}\right) f'' + \frac{W_e}{2} f''^2\right], f(\eta) = 0, \theta(\eta\ ) = 1, \varphi(\eta) = 1, \varepsilon(\eta) = 1\ at\ \ \eta = 0, \tag{13}$$

$$f'(\eta) = 0, \theta(\eta) = 0, \varphi(\eta) = 0, \varepsilon(\eta) = 0\ \ at\ \eta \to \infty.$$

Here $f' = \frac{\partial f}{\partial y}, f'' = \frac{\partial^2 f}{\partial y^2}, f''' = \frac{\partial^3 f}{\partial y^3}, \theta' = \frac{\partial \theta}{\partial y}, \theta'' = \frac{\partial^2 \theta}{\partial y^2}, \varphi' = \frac{\partial \varphi}{\partial y}, \varphi'' = \frac{\partial^2 \varphi}{\partial y^2},\ \varepsilon' = \frac{\partial \varepsilon}{\partial y}$ and $\varepsilon'' = \frac{\partial^2 \varepsilon}{\partial y^2}$. The physical parameters of the above equations such as P_e denotes the bioconvection Peclet number, P_r Prandtl number, λ_1 the slip velocity parameter, W_e the local Weissenberg number, E_c the local Eckert number, M the magnetic parameter, R the radiation parameter, λ local mixed convection parameter, K_p the porosity parameter, N_t the thermophoresis parameter, N_b the Brownian motion parameter, Q the heat generation parameter, S_c the Schmidt number, G the chemical reaction parameter, L_b the bioconvection Lewis number, B the motile density number, R_b the Rayleigh number, N_r. The buoyancy ratio parameter and Ω the microorganism concentration difference parameter. These parameters are valued such as:

$$P_e = \frac{bW_c}{D_m}, P_r = \frac{\vartheta}{\alpha}, \lambda_1 = \lambda_1\sqrt{\frac{a}{\vartheta}}, W_e = \mathrm{r}x\sqrt{\frac{2a^3}{\vartheta}}, E_c = \frac{(ax)^2}{c_p(T_w - T_\infty)}, M = \frac{\sigma B_o^2}{\rho a}, R = \frac{16\sigma^* T_\infty^3}{3kk^*},$$

$$\lambda = \frac{G_r}{R_x^2}, G_r = \frac{\beta g(1-C_\infty)}{\vartheta_f^2}, K_p = \frac{\vartheta}{ka}, N_t = \frac{\tau D_T(T_w - T_\infty)}{T_\infty \vartheta}, N_b = \frac{\tau D_B(C_w - C_\infty)}{\vartheta}, Q = \frac{Q_o}{\rho c_p a}, G = \frac{k_r}{a},$$

$$S_c = \frac{\vartheta}{D_B}, L_b = \frac{\vartheta}{D_m}, B = \frac{e_2}{e_1}, R_b = \frac{\gamma(n_w - n_\infty)(\rho_m - \rho_f)}{\beta\rho_f(1-C_\infty)(T_w - T_\infty)}, \Omega = \frac{n_\infty}{n_w - n_\infty}, N_r = \frac{\gamma(C_w - C_\infty)(\rho_p - \rho_f)}{\beta\rho_f(T_w - T_\infty)}.$$

These results are commonly expressed in terms of the nondimensional skin-friction coefficient. C_f, the local Sherwood number Sh_x, and the local Nusselt number Nu_x. For physical dimensionless parameter is taken [33].

$$C_f R_e^{\frac{1}{2}} = -\left[\left(1 + \frac{1}{\beta}\right) f''(0) + \frac{W_e}{2} f''^2(0)\right], Nu_x R_e^{-\frac{1}{2}} = -(1+R)\theta'(0), \tag{14}$$

$$Sh_x R_e^{-\frac{1}{2}} = -\varphi'(0).$$

3 I NUMERICAL METHODS

The system of ODEs from eq (9) – (13) with boundary condition (14) is solved numerically by using the bvp4c method. The error from the bvp4c method is 10^{-5} which is very small. And in which selection of an initial guess is easy and error is detected easily in this method. Introduce new variables for transforming ODEs into first-order differential equations such as $f = y_1, f' = y_2, f'' = y_3, \theta = y_4, \theta' = y_5, \varphi = y_6, \varphi' = y_7$, $\varepsilon = y_8, \varepsilon' = y_9$, and the first-order differential equation is

$$y_1' = y_2,$$

$$y_2' = y_3,$$

$$y_3' = \frac{1}{\left(1+\frac{1}{\beta}\right)+y_3 * W_e}\left[y_2^2 + k_p * y_2 + M * y_2 - \lambda(y_4 - N_r * y_6 - R_b * y_8\right],$$

$$y_4' = y_5,$$

$$y_5' = \frac{-P_r}{1+R}\left[N_b * y_5 * y_7 + N_t^2 * y_5^2 + E_c\left[\left(1 + \frac{1}{\beta}\right) * y_3^2 + \frac{W_e}{2} * y_3^3\right] + Q * y_4 + y_1 * y_4\right],$$

$$y_6' = y_7,$$

$$y_7' = -\frac{N_t}{N_b} * y_5' + G * S_c * y_6 - S_c * y_1 * y_7,$$

$$y_8' = y_9,$$

$$y_9' = L_b(y_2 * y_8 - y_1 * y_9 + B * y_2) + P_e(y_7'(y_8 + \Omega) + y_9 * y_7),$$

The corresponding boundary conditions are

$$y_1 = 0, y_2 = 1 + \lambda_1\left[\left(1 + \frac{1}{\beta}\right) * y_3 + \frac{W_e}{2} * y_3^2\right], y_4 = 1, y_6 = 1, y_8 = 1 \ \ at\ \eta = 0,$$

$$y_2 = 1, y_4 = 0, y_6 = 0, y_8 = 0 \ \ as\ \eta \to \infty.$$

4 l RESULTS AND ANALYSIS

Present the model of non-Newtonian fluid over a porous sheet with the impact of various parameters on momentum, energy, concentration, and motile density equation. The numerical results are given below. Table 1 shows the present work compared with previous work, in which little error occurs because we solve the model by adding the value of buoyancy and Raleigh term. Table 2 shows the impact of physical parameters on skin friction, Nusselt number, and Sherwood number. Analyze the effect of various parameters on fluid such as velocity, temperature, concentration, and motile density of fluid. The velocity profile examined the impact of parameters such as buoyancy ratio, magnetic field, porous medium, Rayleigh number, and Weissenberg number. In the energy profile study, the impact of various parameters such as Brownian motion parameter, thermophoresis, Eckert number, thermal radiation, and buoyancy ratio. For concentration and bioconvection profile the effect of parameters such as chemical reaction, Eckert number, Brownian and thermophoresis parameters, Lewis number, buoyancy ratio, Schmidt number, and heat source impact respectively.

Table 1. Compare the Nusselt and Sherwood present results with Yousef [33].

N_b	**Yousef [33]**	**Present**
0.1	0.476439	0.4331
0.3	0.342991	0.3537
0.5	0.266807	0.2813

Table 2. The numerical value of local skin friction number, Nusselt number, and Sherwood number for different parameters.

M	R_b	N_r	w_e	N_t	N_b	R	G	S_c	$-f''(0)$	$-\theta'(0)$	$-\varphi'(0)$
0.2	0.1	0.1	0.5	0.1	0.5	0.2	0.2	0.7	0.9864		
0.4									1.0602		
0.6									1.0136		
	0.1								0.9864		
	0.3								1.0290		
	0.5								1.0729		
		0.1							0.9864	0.1805	
		0.3							1.0319	0.1772	
		0.5							1.0784	0.1739	
			0.1						0.8071		
			0.2						0.8143		

			0.5						0.8382		
				0.1						0.2161	0.6710
				0.2						0.1708	0.7187
				0.3						0.1434	0.7528
					0.1					0.4331	
					0.3					0.3537	
					0.5					0.2813	
						0.1				0.2784	0.6828
						0.2				0.2813	0.6710
						0.3				0.2824	0.6617
							0.2				0.6710
							0.4				0.7838
							0.6				0.8801
								0.3			0.4376
								0.5			0.5626
								0.7			0.6710

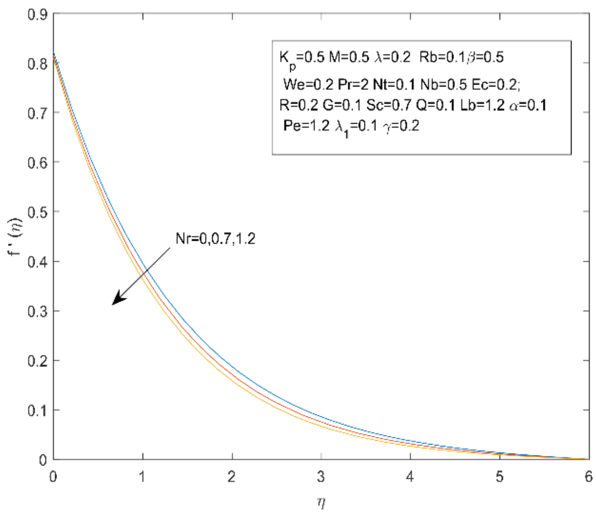

Fig 2(a)

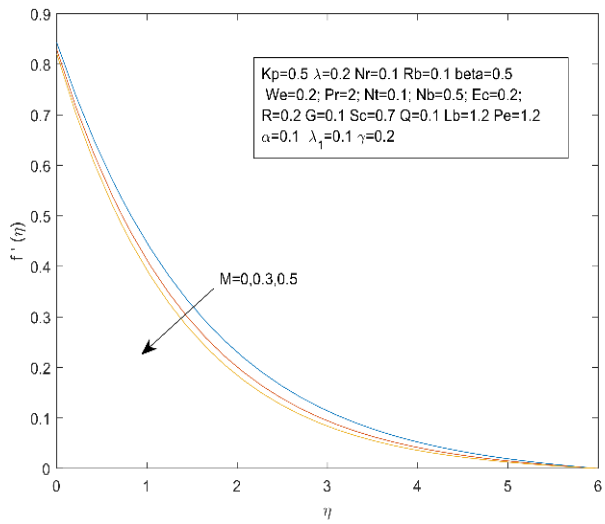

Fig 2(b)

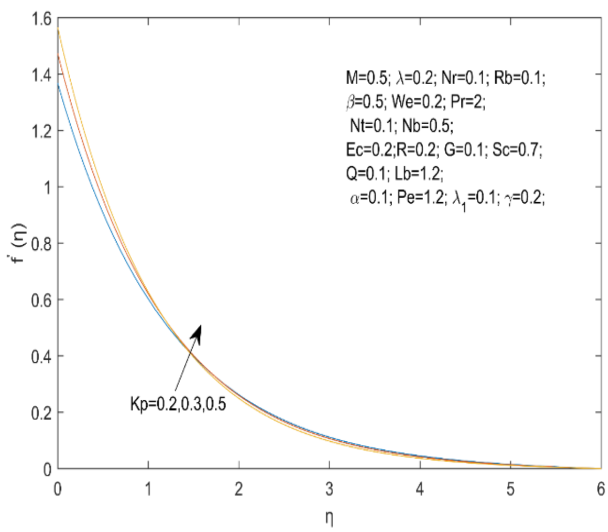

Fig 2(c)

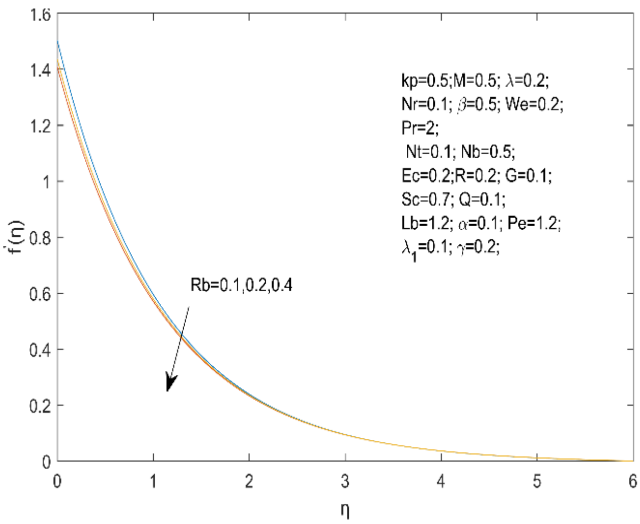

Fig 2(d)

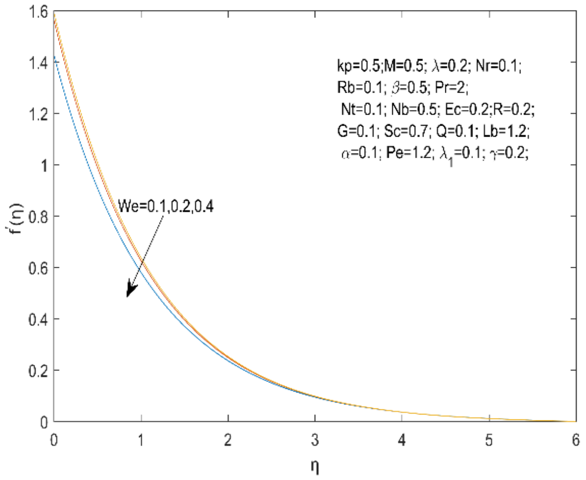

Fig 2(e)

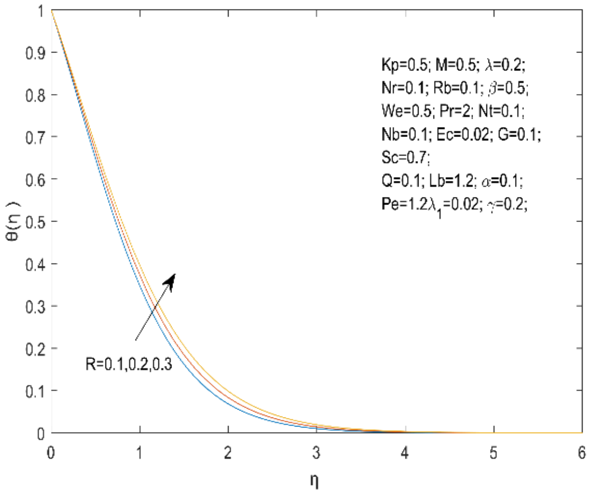

Fig 3(a)

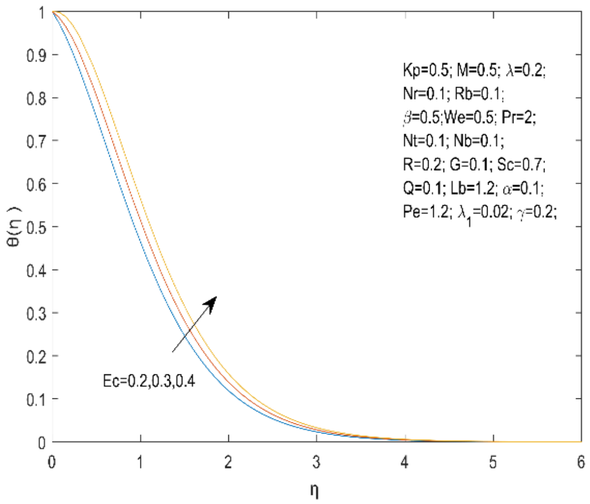

Fig 3(b)

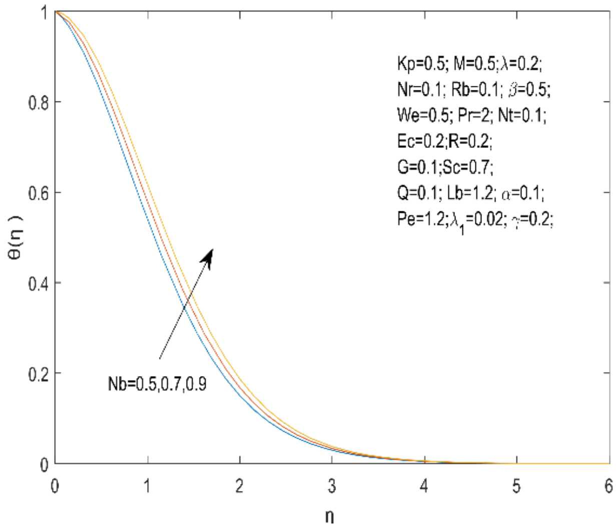

Fig 3(c)

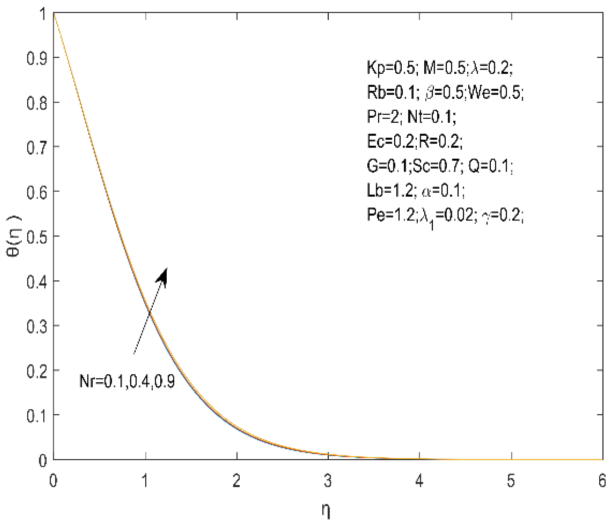

Fig 3(d)

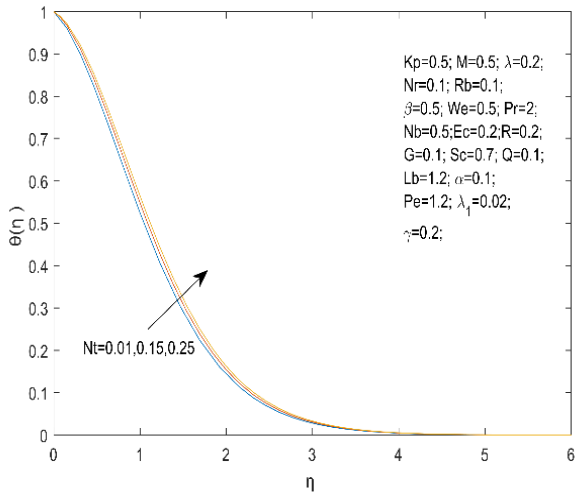

Fig 3(e)

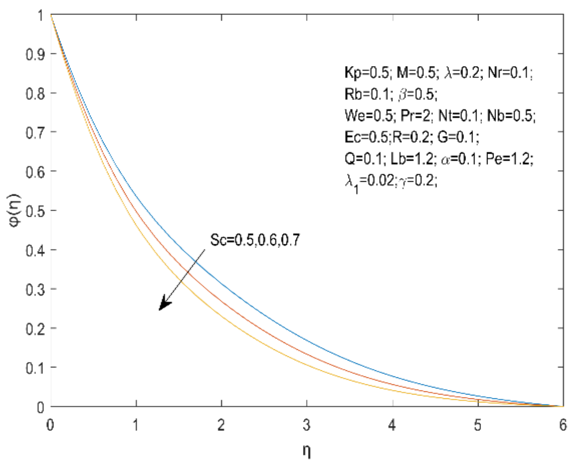

Fig 4(a)

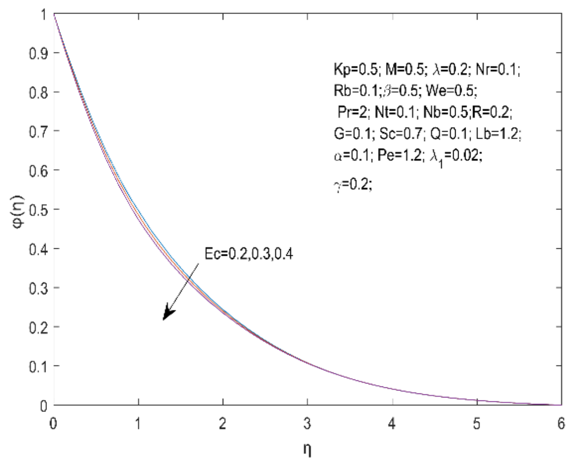

Fig 4(b)

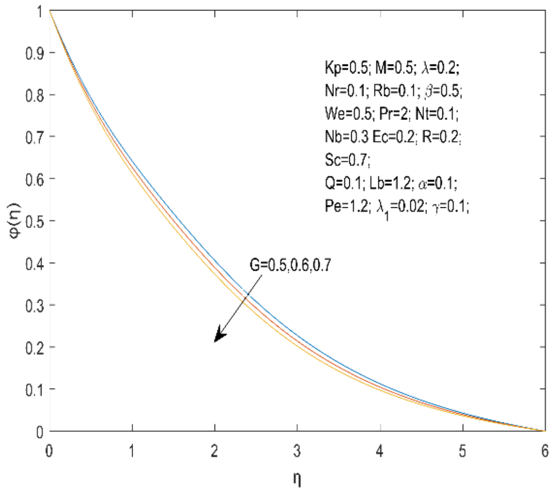

Fig 4(c)

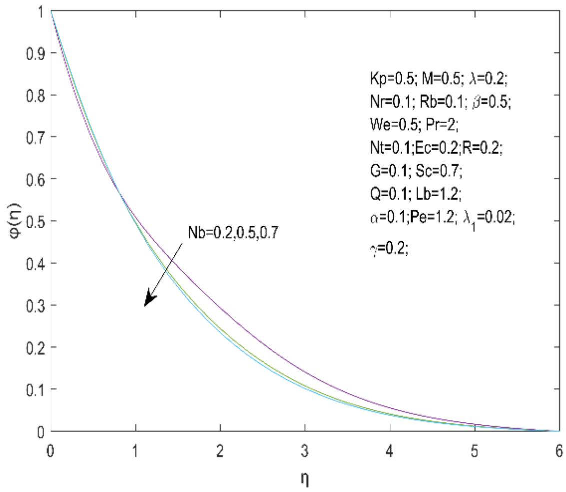

Fig 4(d)

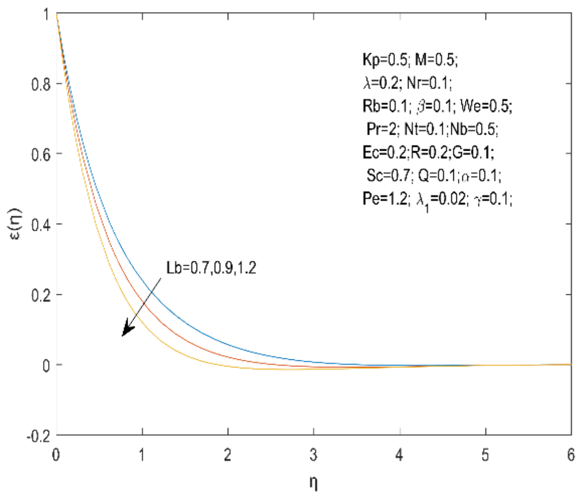

Fig 5(a)

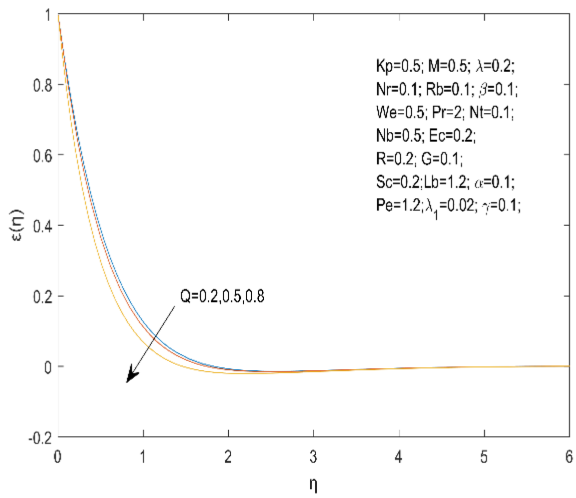

Fig 5(b)

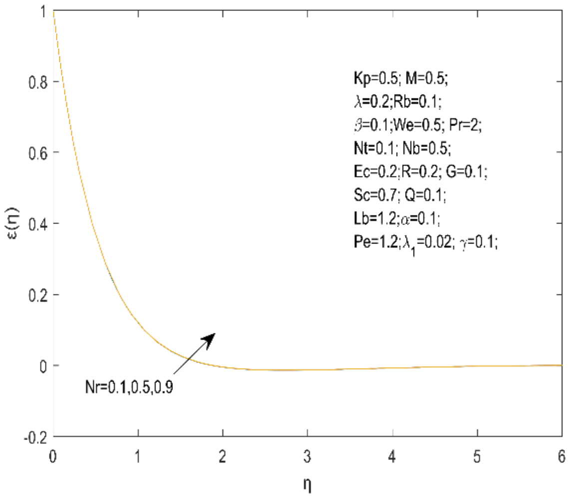

Fig 5(c)

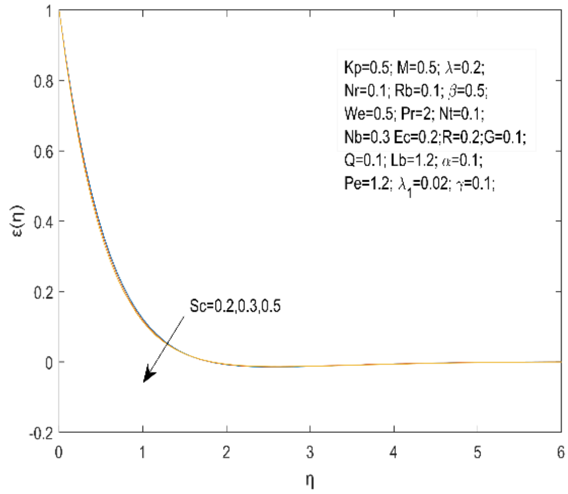

Fig 5(d)

5 | DISCUSSION

Now, the details of the result are mentioned below briefly, in which the profile is impacted by various parameters. We discussed the four profiles: momentum boundary layer, energy, concentration, and bioconvection profile. Fig 2(a) shows the impact of N_r on the velocity profile. The value of N_r The velocity decreases due to drag force increase, and boundary layer thickness also increases due to N_r. Fig 2(b) to observe variations in M influence the velocity $f'(\eta)$. A slight increase in the magnetic number M is shown to result in a decrease in the velocity and an increase in the corresponding boundary layer thickness. This demonstrates how the magnetic effect behaves generally. Fig 2(c) shows the impact of k_p on the velocity profile. The value of k_p Increases then velocity increases due to drag force decrease, and boundary layer thickness also decreases. Fig 2(d) shows the impact of R_b on the velocity profile. The value of R_b Increases then velocity decreases due to drag force increase. Fig 2(e) shows the impact of W_e The local Weissenberg number on the velocity profile. The local Weissenberg number causes the velocity to decrease when the increment of the local Weissenberg number. Fig 3(a) shows the impact of thermal radiation R on the dimensionless temperature profile $\theta(\eta)$. It is examined that as R, grows, so energy profile decreases, and the thickness of the boundary layer increases. Fig 3(b) shows the impact of the viscous dissipation variable Eckert number E_c on the dimensionless temperature profile $\theta(\eta)$. It is examined that as E_c, grows, and so does $\theta(\eta)$ and the thickness of the boundary layer. When the dissipation increases the fluids, thermal conductivity improves enhancing the width of the energy boundary layer. The Brownian motion N_b Impacts the energy curve in Fig 3(c). The rate of nanoparticles is directly related to heat due to N_b. The temperature increases provide the nanoparticles greater kinetic energy, which causes them to move more quickly. In Fig 3(d) the buoyancy ratio parameter N_r indicates the influence of parameter N_r on the dimensionless energy $\theta(\eta)$. The curves of this figure indicate that an increment in the parameter N_r increases the $\theta(\eta)$. In Fig 3(e) to examine the change in the dimensionless temperature $\theta(\eta)$ generated by the thermophoresis parameter N_t. The effect raises the fluid's temperature because heated particles are drawn from hotter to colder regions. The radiation parameter is shown in Fig 3(e). An increase in the radiation factor causes the temperature profile to rise and the overall thickness of the boundary layer to decrease. Fig 4(a) impact of the Schmidt number S_c on the dimensionless concentration profile $\varphi(\eta)$ is depicted in this sketch. $\varphi(\eta)$ is increased for S_c boosting values. Higher Schmidt numbers result in slower mass diffusion, which lowers the concentration of nanoparticles. This is because mass diffusivity and Schmidt number have an inverse relationship. The Fig 4(b) influence of the E_c on the concentration profile $\varphi(\eta)$ demonstrates that a decrease in $\varphi(\eta)$ corresponds to an increase in E_c. The impact of the chemical reaction parameter G on the nanoparticle concentration is shown in Fig 4(c). The parameter G value and boundary layer thickness both marginally increase with decreasing nanoparticle concentration dispersion. A major chemical reaction parameter denotes an impressive pace of chemical transformation between the molecules of the nanofluid, which causes the concentration of the nanofluid to rise slowly. To illustrate the influence of the Brownian motion factor N_b on $\varphi(\eta)$ in Fig 4(d) is presented. $\varphi(\eta)$ decreases due to an incline in N_b. The boundary layer fluid physically warms up due to Brownian motion. As indicated in Fig 5(a) the micro gyrotactic density $\varepsilon(\eta)$ declines for the bioconvection Lewis number L_b. Greater values of L_b Indicate a reduction in the motile microorganism diffusivity which results in a smaller value of $\varepsilon(\eta)$. As shown in Fig 5(b) the mass stratification parameter Q leads to a decline in the micro gyrotactic density $\varepsilon(\eta)$ and boundary layer thickness rises slightly. The Fig 5(c) shows the buoyancy ratio parameter. N_r affects the $\varepsilon(\eta)$ Fluctuation. The motile density profile $\varepsilon(\eta)$ rises with an increase in N_r and boundary layer thickness decreases. The impact of the Schmidt number S_c on the $\varepsilon(\eta)$ is illustrated in Fig. 5(d). The micro gyrotactic density $\varepsilon(\eta)$ decreases as S_c values increase.

6 | CONCLUSION

In this article, the two-dimensional bioconvection and chemical reaction impact on the Casson-Williamson nanofluid has been analyzed. This indicates that with the rise in the porosity parameter k_p, the velocity profile increases and decreases with the bioconvection Rayleigh parameter R_b. The results also show that an increased magnetic number M produces a higher value for the skin friction coefficient. Also, a greater buoyancy ratio N_r, Eckert number E_c, and the thermal radiation parameter R, where these parameters increase the heat transfer. On the other hand, both buoyancy ratio N_r and radiation R have increased the local Nusselt number which means that enhances the loss of heat. The concentration profile diminishes with an increment of Schmidt's number S_c and chemical reaction parameter G along with the Brownian motion parameter N_b Indicating that these parameters oppose mass transfer. Additionally, the motile density profile is reduced as the bioconvection Lewis's parameter L_b Increases and heat generation parameter Q increases. However, when the buoyancy ratio parameter N_r Increases, it decreases the boundary layer thickness while increasing the motile density; meanwhile, the motile density is decreased with an increase in the Schmidt number S_c . Lastly, the value of skin friction decreases with an increase in the magnetic factor and the Nusselt number increases with values of heat generation, showing the interaction between magnetic forces, heat generation, and fluid dynamics. The present results are compared with those reported by Yousef [33], where a good agreement is found. For any value of, the results show minor deviations only, confirming reliability and accuracy in the present analysis.

Future research on Casson-Williamson fluid can be done on its industrial applications to complex processes, this may entail biomedical fluid dynamics, petroleum extraction, and food processing. Additionally, artificial intelligence and optimization techniques using genetic algorithms or learning machines can further improve the predictive models and control the behaviors of fluids in real-time applications. This is further compared in the values of the Nusselt number for the study conducted in the current research with those found by earlier studies, and it is concluded that the values of the Nusselt number in a Casson-Williamson fluid feature considerable variation as dependent on flow conditions and the inclusion of factors. Improvement constitutes the fact that a proposed model produces better thermal performance; hence there is the possibility of achieving better efficiency in the context of transferring heat in practice as compared to older models.

Acknowledgment: We are thankful to the editors and anonymous reviewers for their constructive suggestions.

Author Contributions: Conceptualization, A.R, J.A.J; methodology, A.R; software, J.A.J; validation, A.R; investigation, J.A.R., A.R; data curation, A.R; writing—original draft preparation, A.R; writing—review and editing, J.A.J. Author has read and agreed to the published version of the manuscript.

Declaration of Conflicting Interest: The author(s) declared no potential conflicts of interest with respect to the research, authorship, and/or publication of this article.

Funding: The author(s) received no financial support for the research, authorship, and/or publication of this article.

Data Availability Statement: Data that supports the findings of this study are available on request from the corresponding author.

Plagiarism Statement: This article was scanned by the plagiarism program. No plagiarism was detected.

Disclaimer/Publisher's Note: The statements, opinions, and data contained in all publications are solely those of the individual author(s) and contributor(s) and not of publisher "AGASR" and/or the editor(s). The Publisher AGASR and/or the editor(s) disclaim responsibility for any injury to people or property resulting from any ideas, methods, instructions, or products referred to in the content.

REFERENCES

[1] "Laminar sheet-flow," *Eos Trans. Am. Geophys. Union*, vol. 15, no. 2, pp. 393–404, Jun. 1934, doi: 10.1029/TR015i002p00393.

[2] W. A. Khan and I. Pop, "Boundary-layer flow of a nanofluid past a stretching sheet," *Int. J. Heat Mass Transf.*, vol. 53, no. 11–12, pp. 2477–2483, May 2010, doi: 10.1016/j.ijheatmasstransfer.2010.01.032.

[3] O. D. Makinde and A. Aziz, "Boundary layer flow of a nanofluid past a stretching sheet with a convective boundary condition," *Int. J. Therm. Sci.*, vol. 50, no. 7, pp. 1326–1332, Jul. 2011, doi: 10.1016/j.ijthermalsci.2011.02.019.

[4] M. Hassani, M. Mohammad Tabar, H. Nemati, G. Domairry, and F. Noori, "An analytical solution for boundary layer flow of a nanofluid past a stretching sheet," *Int. J. Therm. Sci.*, vol. 50, no. 11, pp. 2256–2263, Nov. 2011, doi: 10.1016/j.ijthermalsci.2011.05.015.

[5] S. Nadeem *et al.*, "Numerical computations for Buongiorno nano fluid model on the boundary layer flow of viscoelastic fluid towards a nonlinear stretching sheet," *Alex. Eng. J.*, vol. 61, no. 2, pp. 1769–1778, Feb. 2022, doi: 10.1016/j.aej.2021.11.013.

[6] A. Dawar, Z. Shah, A. Tassaddiq, S. Islam, and P. Kumam, "Joule heating in magnetohydrodynamic micropolar boundary layer flow past a stretching sheet with chemical reaction and microstructural slip," *Case Stud. Therm. Eng.*, vol. 25, p. 100870, Jun. 2021, doi: 10.1016/j.csite.2021.100870.

[7] G. B.J., M. Umeshaiah, B. C. Prasannakumara, S. N.S., and M. Archana, "Impact of nonlinear thermal radiation on magnetohydrodynamic three dimensional boundary layer flow of Jeffrey nanofluid over a nonlinearly permeable stretching sheet," *Phys. Stat. Mech. Its Appl.*, vol. 549, p. 124051, Jul. 2020, doi: 10.1016/j.physa.2019.124051.

[8] S. Sindhu and B. J. Gireesha, "Scrutinization of unsteady non-Newtonian fluid flow considering buoyancy effect and thermal radiation: Tangent hyperbolic model," *Int. Commun. Heat Mass Transf.*, vol. 135, p. 106062, Jun. 2022, doi: 10.1016/j.icheatmasstransfer.2022.106062.

[9] A. Hafeez, M. Yasir, M. Khan, M. Y. Malik, and A. S. Alqahtani, "Buoyancy effect on the chemically reactive flow of Cross nanofluid over a shrinking surface: Dual solution," *Int. Commun. Heat Mass Transf.*, vol. 126, p. 105438, Jul. 2021, doi: 10.1016/j.icheatmasstransfer.2021.105438.

[10] P. Mayeli and G. J. Sheard, "Buoyancy-driven flows beyond the Boussinesq approximation: A brief review," *Int. Commun. Heat Mass Transf.*, vol. 125, p. 105316, Jun. 2021, doi: 10.1016/j.icheatmasstransfer.2021.105316.

[11] G. Sandhya, G. Sarojamma, P. V. Satya Narayana, and B. Venkateswarlu, "Buoyancy forces and activation energy on the MHD radiative flow over an exponentially stretching sheet with second-order slip," *Heat Transf.*, vol. 50, no. 1, pp. 784–800, Jan. 2021, doi: 10.1002/htj.21904.

[12] S.-J. Mei and C. Yuan, "Urban buoyancy-driven air flow and modelling method: A critical review," *Build. Environ.*, vol. 210, p. 108708, Feb. 2022, doi: 10.1016/j.buildenv.2021.108708.

[13] A. K. Pandey *et al.*, "Insight into the relationship between non-linear mixed convection and thermal radiation: The case of Newtonian fluid flow due to non-linear stretching," *Propuls. Power Res.*, vol. 12, no. 1, pp. 153–165, Mar. 2023, doi: 10.1016/j.jppr.2022.11.002.

[14] M. Awais, T. Salahuddin, and S. Muhammad, "Evaluating the thermo-physical characteristics of non-Newtonian Casson fluid with enthalpy change," *Therm. Sci. Eng. Prog.*, vol. 42, p. 101948, Jul. 2023, doi: 10.1016/j.tsep.2023.101948.

[15] S. Abbas, Z. U. Nisa, M. Nazar, M. Amjad, H. Ali, and A. Z. Jan, "Application of Heat and Mass Transfer to Convective Flow of Casson Fluids in a Microchannel with Caputo–Fabrizio Derivative Approach," *Arab. J. Sci. Eng.*, vol. 49, no. 1, pp. 1275–1286, Jan. 2024, doi: 10.1007/s13369-023-08351-1.

[16] Z. Shah *et al.*, "Computational intelligence paradigm with Levenberg-Marquardt networks for dynamics of Reynolds nanofluid model for Casson fluid flow," *Tribol. Int.*, vol. 191, p. 109180, Mar. 2024, doi: 10.1016/j.triboint.2023.109180.

[17] E. N. Thabet, A. M. Abd-Alla, H. A. Hosham, and S. M. M. El-Kabeir, "Cattaneo-Christov heat and mass fluxes model of Casson fluid employing non-Fourier double diffusion theories with ion slip and Hall effects," *Ain Shams Eng. J.*, vol. 15, no. 4, p. 102618, Apr. 2024, doi: 10.1016/j.asej.2023.102618.

[18] M. Aneja, A. Chandra, and S. Sharma, "Natural convection in a partially heated porous cavity to Casson fluid," *Int. Commun. Heat Mass Transf.*, vol. 114, p. 104555, May 2020, doi: 10.1016/j.icheatmasstransfer.2020.104555.

[19] H. R. Kataria and H. R. Patel, "Radiation and chemical reaction effects on MHD Casson fluid flow past an oscillating vertical plate embedded in porous medium," *Alex. Eng. J.*, vol. 55, no. 1, pp. 583–595, Mar. 2016, doi: 10.1016/j.aej.2016.01.019.

[20] P. Jalili, S. M. Sharif Mousavi, B. Jalili, P. Pasha, and D. D. Ganji, "Thermal evaluation of MHD Jeffrey fluid flow in the presence of a heat source and chemical reaction," *Int. J. Mod. Phys. B*, vol. 38, no. 08, p. 2450113, Mar. 2024, doi: 10.1142/S0217979224501133.

[21] Y. Dharmendar Reddy, B. Shankar Goud, K. S. Nisar, B. Alshahrani, M. Mahmoud, and C. Park, "Heat absorption/generation effect on MHD heat transfer fluid flow along a stretching cylinder with a porous medium," *Alex. Eng. J.*, vol. 64, pp. 659–666, Feb. 2023, doi: 10.1016/j.aej.2022.08.049.

[22] A. Mirzaei, P. Jalili, M. D. Afifi, B. Jalili, and D. D. Ganji, "Convection heat transfer of MHD fluid flow in the circular cavity with various obstacles: Finite element approach," *Int. J. Thermofluids*, vol. 20, p. 100522, Nov. 2023, doi: 10.1016/j.ijft.2023.100522.

[23] B. Kada *et al.*, "Significance of gyrotactic microorganism and bioconvection analysis for radiative Williamson fluid flow with ferromagnetic nanoparticles," *Therm. Sci. Eng. Prog.*, vol. 39, p. 101732, Mar. 2023, doi: 10.1016/j.tsep.2023.101732.

[24] R. Ellahi, A. Zeeshan, A. Waheed, N. Shehzad, and S. M. Sait, "Natural convection nanofluid flow with heat transfer analysis of carbon nanotubes–water nanofluid inside a vertical truncated wavy cone," *Math. Methods Appl. Sci.*, vol. 46, no. 10, pp. 11303–11321, Jul. 2023, doi: 10.1002/mma.7281.

[25] M. Shoaib and T. Javed, "MHD radiative natural convective heat transfer enhancement for Casson nanofluid flow on a horizontal circular cylinder," *J. Comput. Sci.*, vol. 78, p. 102257, Jun. 2024, doi: 10.1016/j.jocs.2024.102257.

[26] B. Iftikhar, M. Arshad Siddiqui, and T. Javed, "Dynamics of magnetohydrodynamic and ferrohydrodynamic natural convection flow of ferrofluid inside an enclosure under non-uniform magnetic field," *Alex. Eng. J.*, vol. 66, pp. 523–536, Mar. 2023, doi: 10.1016/j.aej.2022.11.011.

[27] S. Li *et al.*, "Insight into the heat transfer across the dynamics of Burger fluid due to stretching and buoyancy forces when thermal radiation and heat source are significant," *Pramana*, vol. 97, no. 4, p. 196, Nov. 2023, doi: 10.1007/s12043-023-02678-y.

[28] B. S. Goud, P. Srilatha, D. Mahendar, T. Srinivasulu, and Y. Dharmendar Reddy, "Thermal radiation effect on thermostatically stratified MHD fluid flow through an accelerated vertical porous plate with viscous dissipation impact," *Partial Differ. Equ. Appl. Math.*, vol. 7, p. 100488, Jun. 2023, doi: 10.1016/j.padiff.2023.100488.

[29] T. Hayat, A. Razaq, S. A. Khan, and S. Momani, "Soret and Dufour impacts in entropy optimized mixed convective flow," *Int. Commun. Heat Mass Transf.*, vol. 141, p. 106575, Feb. 2023, doi: 10.1016/j.icheatmasstransfer.2022.106575.

[30] S. Nadeem, B. Ishtiaq, J. Alzabut, and H. A. Ghazwani, "Entropy generation for exact irreversibility analysis in the MHD channel flow of Williamson fluid with combined convective-radiative boundary conditions," *Heliyon*, vol. 10, no. 4, p. e26432, Feb. 2024, doi: 10.1016/j.heliyon.2024.e26432.

[31] A. R. Ajaykumar, P. Kumar, F. Almeida, B. Nagaraja, and Q. Al-Mdallal, "Sensitivity analysis and response surface methodology for entropy optimization in the exponentially stretching stratified curved sheet for Casson–Williamson nanofluid flow," *Int. J. Thermofluids*, vol. 22, p. 100668, May 2024, doi: 10.1016/j.ijft.2024.100668.

[32] N. Gomathi and D. Poulomi, "Dual solutions of Casson Williamson nanofluid with thermal radiation and chemical reaction," *Numer. Heat Transf. Part Appl.*, pp. 1–24, Mar. 2024, doi: 10.1080/10407782.2024.2326980.

[33] N. S. Yousef, A. M. Megahed, N. I. Ghoneim, M. Elsafi, and E. Fares, "Chemical reaction impact on MHD dissipative Casson-Williamson nanofluid flow over a slippery stretching sheet through porous medium," *Alex. Eng. J.*, vol. 61, no. 12, pp. 10161–10170, Dec. 2022, doi: 10.1016/j.aej.2022.03.032.

[34] S. M. Atif, S. Hussain, and M. Sagheer, "Magnetohydrodynamic stratified bioconvective flow of micropolar nanofluid due to gyrotactic microorganisms," *AIP Adv.*, vol. 9, no. 2, p. 025208, Feb. 2019, doi: 10.1063/1.5085742.